Compact Superdirective Electric Dipole Array for Far-field Measurement in a Semi-Anechoic Environment

Frédéric Munoz, Serge Bories, Mathieu Caillet, Laurent Lombard, Jean-François Pintos

Compact Superdirective Electric Dipole Array for Far-field Measurement in a Semi-Anechoic Environment

Frederic Munoz, Serge Bories, Mathieu Caillet, Laurent Lombard, Jean-François Pintos
CEA-LETI, Grenoble, France, emails: frederic.munoz@cea.fr, serge.bories@cea.fr, jean-francois.pintos@cea.fr

***Abstract*—This paper investigates the theory of superdirective arrays with electric dipoles as elements placed over a metallic reflector. A practical design of such antenna array is designed with a primary concern on the antenna compactness while keeping a relatively wide matching bandwidth. This antenna array, contained in a ka = 1.8 Chu sphere electrical radius, shows a maximum directivity of 11.8 dBi at 80 MHz while being matched over a 15.6 % fractional bandwidth. The proposed antenna is a good candidate for far-field measurements in presence of specular reflection inside an anechoic chamber below its minimal working frequency.**

***Index Terms*—Compact antennas, superdirectivity, anechoic chamber measurements.**

I. Introduction

Far-field measurements of an antenna inside an anechoic chamber in the VHF-UHF frequency bands are performed at the expensive cost of increasing the size of the absorbers and the whole size of the facility [1] - [2]. On the absorber side, the use of heavy ferrite tiles can mitigate this issue but at higher cost and a heavier setup. However the demand of miniaturized antenna and its qualification at low frequencies represent an ongoing topic of interest. Therefore solutions to minimize the anechoic chamber reflectivity and improvement to the measurement accuracy in these frequencies are welcomed, especially if such solutions involves no modification of the existing measurement facility, effectively extending its range of utilization.

Degradation of the anechoic chamber reflectivity at low frequencies for a given chamber arise from the specular paths occurring when the absorbers reflectivity degrades with the higher wavelength [3]. Moreover the interaction increases between the positioning setup and the probe antenna or the antenna under test as the frequency decreases. Usual probe antennas in the VHF-UHF frequency range are mostly non directive because of the antenna size constraint. But a directive antenna pointed to the antenna under test will illuminate less the side walls, resulting in less specular multipath coming from them, improving the anechoic chamber reflectivity and reducing the measurement inaccuracies.

A sufficiently compact and directional antenna can be classified as a superdirective antenna [4]. The classical Uzkov limit [5] given for an End-Fire array of isotropic sources relates proportionally the number of element inside the array to the directivity level. Showing that there is, in theory, no limit in the directivity achievable with a given Chu sphere. Nevertheless practical implementation of End-Fire arrays needs effective radiator of finite size to operate. Moreover arrays of more than three elements tend to lead to tolerance issues for the complex amplitude weight to apply at each element. Therefore in this paper, a design of a superdirective array with a metal reflector, a Perfect Electric Conductor (PEC) surface, will be used. It has two major advantages, first it allows for a compact design in the End-Fire direction by reducing the number of real radiating elements. Secondly the reflector isolates the probe from the half space behind the radiating elements (Antenna mast, metallic parts...).

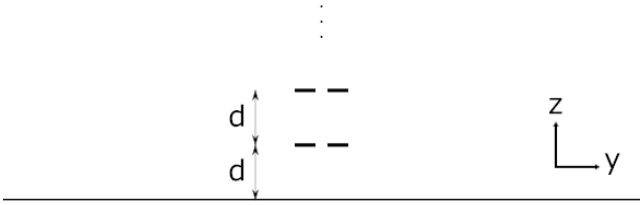

Fig. 1. Illustration: End-Fire array of elementary dipole above a surface.

In this paper, Section II will introduce the problem of electric dipoles above a metallic reflector as a simple system of linear equations giving a directivity limit depending on the amount of antenna elements over the reflective surface. Section III describes the strategy in the radiating elements design and weighting scheme. Finally Section IV is dedicated to the Full-Wave simulation results of the antenna for validation.

II. Electric dipoles over a metallic reflector

Lets assume a problem of electric dipoles over a PEC plane with the dipoles axes parallel to the plane, see Fig. 1. This problem is readily simplified by using the image principle applied to an electric dipole over a PEC surface. The demonstration is similar to the one shown in [6], here for the case of an anti-symmetric array. This gives, by definition, a complex excitation amplitudes A_n link between the array elements. As shown with the following equation:

$$A_n = -A_{-n},\ \forall\ n \in N^*. \tag{1}$$

Each dipole has a far-field pattern $\mathbf{f}_n(\theta, \phi)$. Let's take the Cartesian coordinates with the z-axis as the axis of the End-Fire non-uniform array. The array inter-element distance is d.

For this setup the maximum directivity is obtained for a given direction θ_0 by solving the following system of equations:

$$\sum_{n=1}^{N} a_{0n} h_{mn}(\theta_0, \phi_0) = \sin(mkd\cos\theta_0) \tag{2}$$

a_{0n} are coefficients maximizing the directivity for the θ_0 direction with $a_n = A_n|\mathbf{f}_n(\theta,\phi)|$. k is the free-space wave number and h_{mn} is given in the following equations:

$$h_{mn}(\theta,\phi) = \frac{H_{mn}}{\mathbf{f}_m(\theta,\phi)\cdot\mathbf{f}_n^*(\theta,\phi)} \tag{3}$$

$$\begin{aligned} H_{mn} = \tfrac{1}{4\pi} \int_0^{2\pi}\int_0^{\pi} \mathbf{f}_m(\theta,\phi)\cdot\mathbf{f}_n^*(\theta,\phi)\sin(mkd\cos\theta) \\ \times \sin(nkd\cos\theta)\sin\theta\, d\theta\, d\phi \end{aligned} \tag{4}$$

Solving (2) gives the maximum End-Fire directivity for an anti-symmetric array which then follows the inter-element dependence (1). Finally, the directivity obtained in presence of a infinite ground plane, here a PEC surface, is given by (5).

$$D(\theta_0,\phi_0) = \sum_{n=1}^{N} 2a_{0n}\sin(mkd\cos\theta_0) \tag{5}$$

To illustrate the directivity achieved in the case of an anti-symmetric array created by the reflective surface let's use N elementary electric dipoles as our radiating sources with the following far field radiation pattern for each element:

$$\mathbf{f}_n = \cos\theta\sin\phi\mathbf{e}_\theta + \sin\phi\mathbf{e}_\phi \tag{6}$$

Injecting (6) inside (3), then solving (2) gives the complex amplitude to apply for each element of the array, in order to maximize the directivity in the direction θ_0. Here the the End-Fire direction is the main interest, therefore $\theta_0 = 0$. The following arrays of 1, 2 and 3 elementary electric dipole are computed. Their inter-distance is d with the closest element of the PEC reflector at d as well. An illustration of the scenarios is shown Fig. 1.

The directivity obtained in the End-Fire direction is compared to the directivity obtained for the same array geometry but with elementary magnetic dipole as radiating sources as described in [6].

Fig. 2 the directivity obtained for the 1, 2 and 3 electric dipole(s) over a metallic surface when $d \longrightarrow 0$ is 8.75 dBi, 13.57 dBi and 16.62 dBi respectively, including the surface effect of 3 dB. It can be noticed that the directivity of an electric dipole array is systematically better than a magnetic dipole array. Those values are consistent with results shown in [7] obtained with a generalized Rayleigh quotient maximization process.

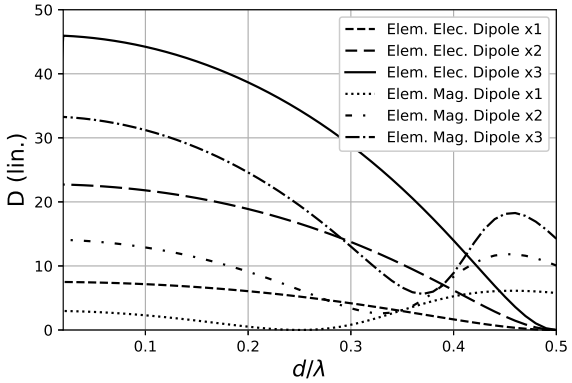

Fig. 2. Elementary (Elem.) Electric/ Magnetic dipole End-Fire array directivity over a PEC surface.

III. Radiating Elements and Weightings

One of the main challenges in superdirective design is the narrowband behaviour of the system [6] [8] [9]. One way to extend the bandwidth consists in the use of Non-Foster elements [10], another way to do it is to rely on a better use of the Chu sphere improving its geometrical array Q-factor [9]. The latter bandwidth improvement method can be done as early as selecting the global shape of the array. In practice a spherical shape would be the best choice to do so but for a large wavelength, e.g. 3.75 m at 80 MHz, this shape leads to a complex realization and manipulation of the antenna array. A cylindrical shape is a good compromise between a planar and spherical shape.

A. Excitation Dipole

The antenna array proposed here is a parasitic array with complex loads optimized for End-Fire directivity. The electrical dipole seen in Fig. 3 is selected to be the feeder and the two others loops are the parasitics elements of the array. Its symmetrical structure is well adapted for an array of elements placed in a cylindrical shape. It provides coupling symmetrically, and if small enough, this element can be translated along the cylinder axis in order to find coupling region where the directivity optimization process do not produce loads with negative real part. Indeed in the array optimization process the powered electric dipole geometrical parameters will be optimized in order to get the high directivity needed while using only passive and realistic loads for the parasitic elements.

B. Horizontal Loops

In order to better fill the cylindrical space, the use of ribbons as radiating elements fulfils this intention pretty well. It is well known [12] that a x-y plane aligned loop with circumference $C = \lambda$ radiates equally in +z and -z direction. Nevertheless for compactness purposes, the loop needs to be smaller. Such miniaturization process leads to a main lobe shift in the radiation pattern in the loop x-y plane like an elementary

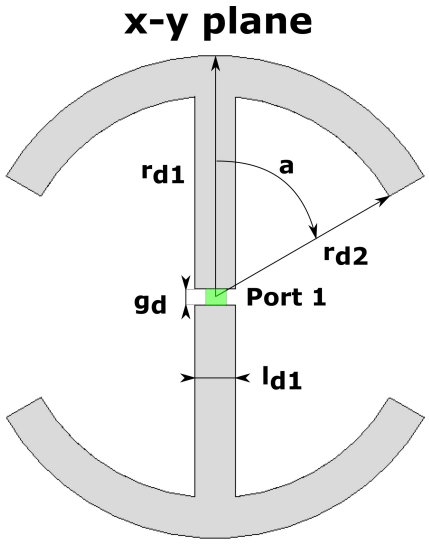

Fig. 3. Excitation dipole geometry.

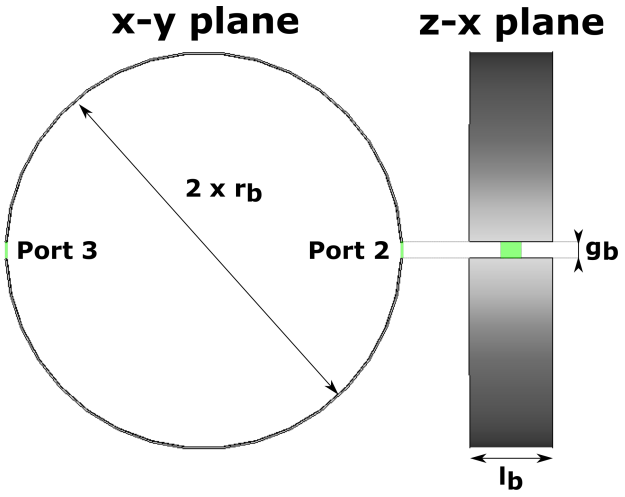

Fig. 4. Ribbon-like loop geometry.

magnetic dipole. The goal is to keep the radiation out of the loop plane. To do so, let's analyze the loop as a two port radiating element which can be optimized in directivity for the +z direction, with the Altshuler method [11] for instance. The radiation characteristics of the loop is evaluated using CST Microwave Studio software.

Fig. 4 illustrates the metallic ribbon-like element geometry. In this study the fixed parameters are $l_b = 10\ cm$, $g_b = 2\ cm$ and the loop thickness which is equal to $2\ mm$. The loop radius vary between $r_b = 30\ cm$ and $r_b = 90\ cm$ and is the major factor in the element compactness.

Fig. 5 shows how the directivity can be maintained in the +z direction by imposing on port 2 and 3 a given set of complex amplitude for each loop circumference. Those weights are displayed in Fig. 6. It can be seen that the two port when symmetrically placed needs to be weighted at the same amplitude with only a relative phase difference. In this

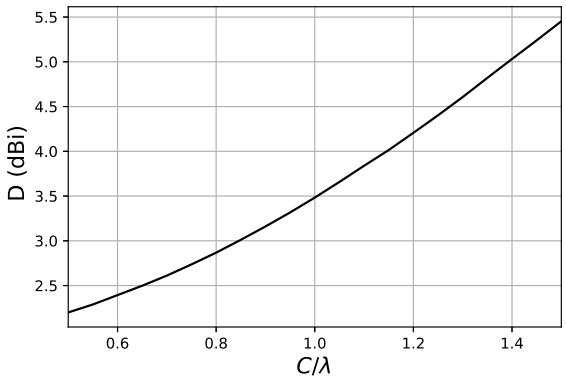

Fig. 5. Directivity in +z axis over the circumference variation.

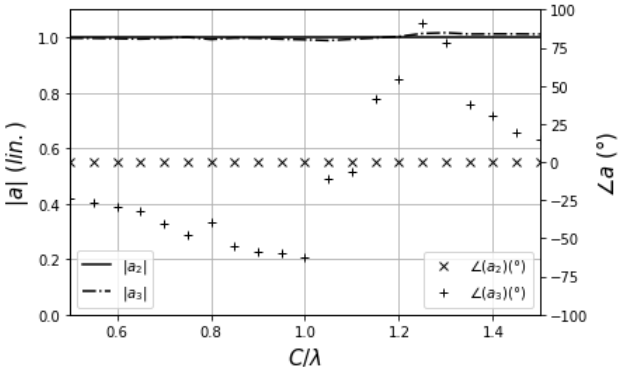

Fig. 6. Port 2 & 3 complex weights over the circumference variation.

study the complex amplitude will be set for the loops in a parasitic manner with discrete loads soldered on PCB at each port. Another way to see this loop setup is to consider the two ports as electric dipoles placed in a broadside manner with complex weight optimized for broadside directivity. A singular point in equiphase is visible on the Fig. 6 at $C = 1.1\lambda$ indicating a short circuit.

The array presented in this work have two compact loops placed in End-Fire fashion with the loops dimensions and separation distances optimized for passive loads and high directivity.

C. Weighting Scheme

A slight modification of the usual superdirective weighting scheme is applied. Since the End-Fire geometry provides the directivity needed, the electric dipole excited can used for coupling optimisation with parasitics elements. The Altshuler method [11] is used to get the complex weight at each port a_i, by choosing the second port as a reference and deducing the relation between every port to the second port with $\frac{a_i}{a_2} = k_i\ \forall\ i \in [1, N]$. By setting a perfect matching on port 1 $b_1 = 0$ the scattering matrix provides the following system:

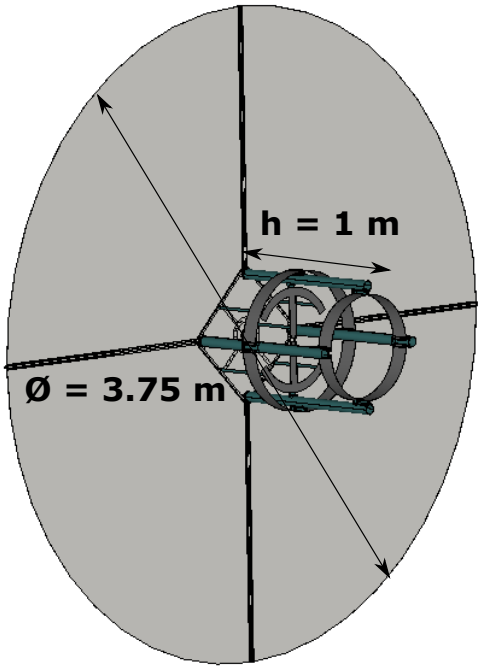

Fig. 7. CST Full-Wave antenna array model.

$$\begin{bmatrix} 0 \\ b_2 \\ \vdots \\ b_N \end{bmatrix} = [S] \begin{bmatrix} 1 \\ a_2 \\ \vdots \\ k_N a_2 \end{bmatrix} \tag{7}$$

Following the equivalence principle [8] between the load Z_i and the reflection coefficient Γ_i obtained with the parameter solution from (7), the loads are deducted with:

$$Z_i = Z_0 \frac{1+\Gamma_i}{1-\Gamma_i} \tag{8}$$

IV. Array Optimization Results

The Full-Wave simulated antenna design is shown Fig. 7. The metallic reflector used in the simulation has a diameter of 1λ giving a value of 3.75 m at the frequency of interest. This reflector is challenging to make and manipulate. But can be made in practice for instance with light-weight sail-like conductive sheets. Structural pylons in PMMA, maintaining the radiating elements, are also integrated in the model shown in Fig. 7.

A. Load and Geometrical Optimization

A 1:2 balun is placed at the feeding dipole, therefore the optimization is made on a $Z_0 = 100\ \Omega$ reference impedance. After an iterative procedure with the model inside the Full-Wave simulator CST, one geometry is selected. It has two loops, the closest one from the reflector is noted loop 1 and the other one is loop 2. For all elements, the distance between the reflector and the element center is noted d. The geometrical parameters are summarised Table I and the associated loads are found in Table II. For each element a $2\ mm$ sheet of aluminium is used, and each port gap has the same length $g_d = g_{b,1/2} = 2\ cm$.

TABLE I
Array Geometrical Parameters

	$r_{d1}\ (cm)$	$r_{d2}\ (cm)$	$l_d\ (cm)$	$d\ (cm)$	$a\ (^\circ)$
Dipole	30	25	5	37.5	30
	$r_b\ (cm)$	$l_b\ (cm)$	$d\ (cm)$	N.C	N.C
Loop 1	40	10	42.5		
Loop 2	30	10	92.5		

TABLE II
Loads Parameters

Port	$R\ (\Omega)$	$L\ (nH)$
1	100	0
2	14.5	211
3	14.5	211
4	0	360
5	0	360

B. Radiation and Impedance Bandwidth

Magnitude of the reflection coefficient $|S_{11}|$ is presented Fig. 8. The matching level lower than -10 dB is obtained between 78.3 MHz and 91.6 MHz, resulting in a fractional bandwidth equal to 15.6 %, centered around 85 MHz. The balun losses around 2 dB can be seen as well.

The directivity maximum value $D = 11.8$ dBi is obtained at the frequency of interest 80 MHz as shown in Fig. 9. The gain and realized gain at 80 MHz are equal to -11.9 dBi. The Harrington [13] limit is also shown in order to illustrate the superdirectivity frequency region obtained. A drop in the antenna efficiency at the maximum directivity is seen with the realized gain and gain, a behaviour expected for an antenna in a superdirectivity regime. Also a drop in the End-Fire directivity is noted, explained by a limited reversal of the antenna pattern, happening due to the PEC reflector finite size.

The radiation pattern at 80 MHz is shown Fig. 10. A good symmetry can be observed for the main lobe in the azimuth and elevation plane with a very low cross polarisation in both plane.

V. Conclusion

In this paper, a straightforward procedure is proposed to obtain the directivity of an array with anti-symmetric properties, for instance with electric dipoles over a PEC surface, showing high directivities obtained with only 2 - 3 elements, respectively 13.57 dBi and 16.62 dBi, owing to the presence of a surface and the image principle. A compact array based on this principle is proposed $ka = 1.8$, with an improved filling of the Chu sphere thanks to ribbon-like loop element, and the near-field matching scheme. A maximum End-Fire directivity of 11.8 dBi is obtained with a large superdirective frequency bandwidth around the frequency of interest 80 MHz. The proposed antenna is well suited as a probe antenna in

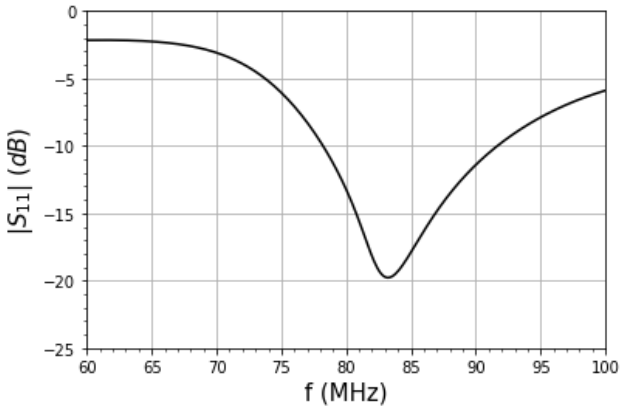

Fig. 8. Magnitude of the reflection coefficient $|S_{11}|$

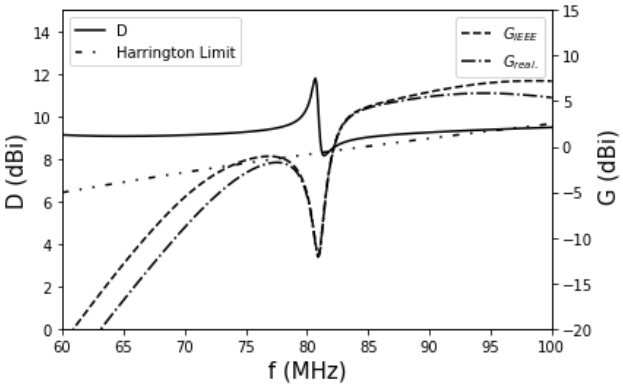

Fig. 9. Simulated Endfire directivity, gain and realized gain of the proposed antenna array.

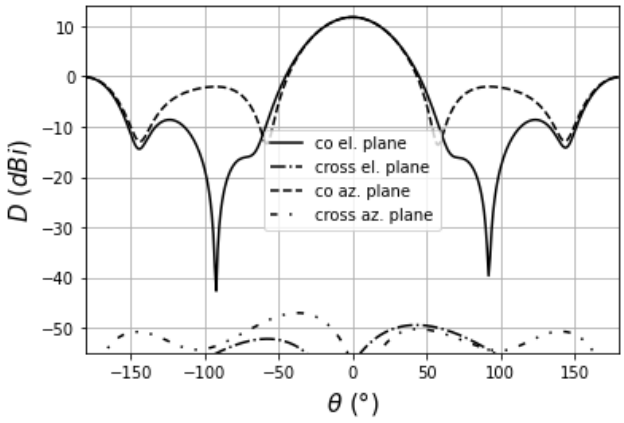

Fig. 10. Simulated directivity at 80 MHz pattern for the elevation (el.) and azimuthal (az.) plane.

the CEA-Leti anechoic chamber below its nominal frequency of 100 MHz. Allowing to minimize the side-walls specular paths thanks to its directivity, compactness and relatively large fractional matching bandwidth of 15.6 %.

ACKNOWLEDGMENT

This work is supported by a public grant overseen by the French National Research Agency and by the French Defense Innovation Agency (ANR-19-ASTR-0006, MEASUREMENt project).

REFERENCES

[1] A. Clemente, S. Bories, J. Pintos, J. Keignart and C. Delaveaud, "Antenna measurements from 50 MHz to millimeter wave frequencies at the CEA-Leti far-field facility," 2017 International Conference on Electromagnetics in Advanced Applications (ICEAA), 2017, pp. 1327-1330, doi: 10.1109/ICEAA.2017.8065519.

[2] G. Le Fur and al., "Implementation of a VHF Spherical Near-Field Measurement Facility at CNES," AMTA 2016, Oct 2016, Austin, United States. ⟨hal-01523536⟩

[3] F. Munoz, S. Bories, M. Caillet, J. -F. Pintos, G. L. Fur and A. Bellion, "Anechoic Chamber Reflectivity Analyses below its minimal frequency using the Matrix Pencil Method," 2021 IEEE Conference on Antenna Measurements & Applications (CAMA), 2021, pp. 165-168, doi: 10.1109/CAMA49227.2021.9703583.

[4] M. Pigeon, C. Delaveaud, L. Rudant, and K. Belmkaddem, "Miniature directive antennas," International Journal of Microwave and Wireless Technologies, vol. 6, no. 1, pp. 45–50, 2014.

[5] A. I. Uzkov, "An approach to the problem of optimum directive antennae design," Comptes Rendus de l'Acad. Sci. l'URSS, vol. 53, no. 1, pp. 35–38, 1946.

[6] O. S. Kim, S. Pivnenko and O. Breinbjerg, "Superdirective Magnetic Dipole Array as a First-Order Probe for Spherical Near-Field Antenna Measurements," in IEEE Transactions on Antennas and Propagation, vol. 60, no. 10, pp. 4670-4676, Oct. 2012, doi: 10.1109/TAP.2012.2207363.

[7] O. Hernández, I. Buldain, I. Ederra, R. W. Ziolkowski and I. Liberal, "Highly-Directive Cross-Polarized Backscatterers Integrated With a Ground Plane," in IEEE Transactions on Antennas and Propagation, vol. 69, no. 10, pp. 6739-6751, Oct. 2021, doi: 10.1109/TAP.2021.3076236.

[8] A. Clemente, M. Pigeon, L. Rudant and C. Delaveaud, "Design of a Super Directive Four-Element Compact Antenna Array Using Spherical Wave Expansion," in IEEE Transactions on Antennas and Propagation, vol. 63, no. 11, pp. 4715-4722, Nov. 2015, doi: 10.1109/TAP.2015.2475617.

[9] O. S. Kim, "Compact First-Order Probe for Spherical Near-Field Antenna Measurements at Low Frequencies," in IEEE Transactions on Antennas and Propagation, vol. 65, no. 7, pp. 3684-3690, July 2017, doi: 10.1109/TAP.2017.2700051.

[10] L. Batel, L. Rudant, J. -F. Pintos, A. Clemente, C. Delaveaud and K. Mahdjoubi, "High directive compact antenna with non-foster elements," 2015 International Workshop on Antenna Technology (iWAT), Seoul, Korea (South), 2015, pp. 381-384, doi: 10.1109/IWAT.2015.7365294.

[11] E. E. Altshuler, T. H. O'Donnell, A. D. Yaghjian and S. R. Best, "A monopole superdirective array," in IEEE Transactions on Antennas and Propagation, vol. 53, no. 8, pp. 2653-2661, Aug. 2005, doi: 10.1109/TAP.2005.851810.

[12] D. H. Werner, "An exact integration procedure for vector potentials of thin circular loop antennas," in IEEE Transactions on Antennas and Propagation, vol. 44, no. 2, pp. 157-165, Feb. 1996, doi: 10.1109/8.481642.

[13] R. Harrington, "On the gain and beamwidth of directional antennas," in IRE Transactions on Antennas and Propagation, vol. 6, no. 3, pp. 219-225, July 1958, doi: 10.1109/TAP.1958.1144605.